Petroleum Science 23 (2026) 730–741

Contents lists available at ScienceDirect

Petroleum Science

journal homepage: www.keaipublishing.com/en/journals/petroleum-science

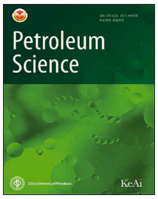

Original Paper

Application of acrylic-based wellbore strengthening material in water-based drilling fluid to stabilize the fractured formation

Kai-He Lv[a,b,c,*], Juan He[a,b,c], Xian-Bin Huang[a,b,c], Jin-Sheng Sun[a,b,c,d]

[a] *State Key Laboratory of Deep Oil and Gas, China University of Petroleum (East China), Qingdao, 266580, Shandong, China*
[b] *School of Petroleum Engineering, China University of Petroleum (East China), Qingdao, 266580, Shandong, China*
[c] *Key Laboratory of Unconventional Oil & Gas Development (China University of Petroleum (East China)), Ministry of Education, Qingdao, 266580, Shandong, China*
[d] *CNPC Engineering Technology R&D Company Limited, Beijing, 102206, China*

ARTICLE INFO

Article history:
Received 2 April 2025
Received in revised form
19 November 2025
Accepted 19 November 2025
Available online 22 November 2025

Edited by Jia-Jia Fei

Keywords:
Wellbore strengthening material
Water-based drilling fluid
Acrylic resin
Acrylic resin enhanced by hydrophobically modified calcium carbonate

ABSTRACT

Wellbore instability is the main challenge encountered during borehole construction, particularly when employing water-based drilling fluid (WBDF) under complex geological conditions. A novel wellbore strengthening material of acrylic resin enhanced by hydrophobically modified calcium carbonate particles (ARH) is synthesized by emulsion polymerization. Transmission electron microscope and particle size analysis reveal that ARH exhibits a spherical structure with a *Z*-average diameter of 277.6 nm. The lap shear strength test shows ARH effectively adheres to two rock slices with a stress of 0.4838 MPa. Uniaxial compressive strength experiments of simulated rock cores verify that ARH can greatly enhance the compressive strength of the simulated core column to 7.1567 MPa. The incorporation of ARH significantly enhances the compressive strength of shale cores, with increases of 18.0620 and 18.9147 MPa compared to those immersed in water and base fluid, respectively. Further microporous membrane plugging experiments show that the filtration losses of 2% ARH in 4% base fluid through 0.1, 0.2, and 0.45 μm microporous membranes are 13.5, 13.2, and 27 mL, respectively, demonstrating excellent plugging capabilities for enhancing wellbore stability. This work generates important theoretical foundations and practical recommendations for wellbore strengthening applications utilizing ARH in complex drilling environments.

1. Introduction

With the advancement of petroleum exploration into deeper formations, the geological conditions encountered in drilling operations have become increasingly complex, significantly raising the probability of encountering fragile formations. These formations typically exhibit loose rock structures, poor cementation, and extensive fractures (Sun et al., 2024a; Zhao et al., 2019; Jiang et al., 2025). Under the combined influence of drilling fluid invasion and in-situ stress release, these conditions readily result in decreased wellbore stability, triggering enlargement, drill pipe sticking, or even wellbore collapse, severely restricting the safe construction and economic efficiency of deep wells. Thus, effectively reinforcing the wellbore wall to maintain wellbore stability has become a critical issue that urgently needs to be resolved in deep drilling operations.

Currently, the commonly used method for wellbore reinforcement is introducing plugging materials into drilling fluids to plug subsurface pores and fractures. Typical plugging agents cover inorganic materials, organic additives, and organic-inorganic composites (Huang et al., 2022; Xu et al., 2023; Feng and Gray, 2017; Lei et al., 2022; Liu et al., 2023). Inorganic plugging agents exhibit high plugging strength due to their inherent rigidity (Sun et al., 2024b; Liu and Ott, 2020; Liu et al., 2025). However, their fixed particle sizes limit their ability to accurately match the varied formation pore and fracture sizes. Organic plugging agents effectively conform to complex fracture and pore structures due to their favorable deformability, but they are disadvantaged by insufficient plugging strength and reduced long-term stability (Yang et al., 2025a; Wang et al., 2024; Luo et al., 2025). Organic and inorganic mixture

---

* Corresponding author.
E-mail address: lkh54321@126.com (K.-H. Lv).
Peer review under the responsibility of China University of Petroleum (Beijing).

https://doi.org/10.1016/j.petsci.2025.11.037
1995-8226/

plugging agents aim to integrate the beneficial properties of these two material types (Xu et al., 2023; Yang et al., 2025b). Nonetheless, because their plugging method primarily relies on physical mixing, their plugging layers are susceptible to migration and instability under continuous drilling fluid circulation, thereby failing to maintain lasting effectiveness. Researchers have investigated the chemical incorporation of inorganic and organic materials to enhance the stability of the wellbore (He et al., 2024; Yang et al., 2024; Tang et al., 2022). Xu et al. (2023) introduced a plugging agent (PANS) with a rigid inorganic internal structure and a flexible organic external shell for WBDF. PANS showed a 71.4% enhancement in blocking performance after thermal aging at 180 °C when it was assessed using sand layers graded from 100 to 120 mesh. Recently, wellbore strengthening materials with chemical adhesive properties have emerged as an innovative research direction (Huang et al., 2023; Zhang et al., 2018; Gu et al., 2004). Wang et al. (2023) prepared a kind of biomimetic wellbore stabilizer (TA-PVA) based on multiple hydrogen bonding, which can adhere to silica microspheres with an adhesion force of 164.46 mN/m.

Inspired by these works, this study develops a kind of acrylic resin enhanced by hydrophobically modified $CaCO_3$ (ARH) as wellbore strengthening material to maintain wellbore stability in fractured formations, integrating the merits of physical blockage, deformation filling, and chemical adhesion. The molecular structure and crystalline form are confirmed by FTIR, solid-state NMR, and XRD analyses. Thermal properties of the prepared ARH are characterized using thermal gravimetric analysis (TGA), while differential scanning calorimetry (DSC) is employed to determine the glass transition temperature. Lap shear strength tests, simulated and real core column compressive strength tests, and microporous membrane plugging experiments confirm that the synthesized ARH could effectively cement wellbore rocks, enhance core mechanical strength, and plug pore fractures, providing a feasible solution for wellbore stabilization.

2. Materials and methods

2.1. Chemicals

Styrene (>99.5%), methyl methacrylate (>99.5%), acrylamide (99%), 3-(isobutene-1-ylcarbonyloxy)propyltrimethoxysilane (KH-570, 97%), and calcium carbonate were all purchased from Macklin. Sodium salt of alkylphenol ether sulfonated succinate ester (OS, 40%) was obtained from Shandong Yousuo Chemical Technology Co., Ltd.

2.2. Hydrophobic modification of calcium carbonate

Hydrophobic modification of calcium carbonate ($HCaCO_3$) was fabricated by following Tang's work (Tang et al., 2014). The original $CaCO_3$ underwent a drying process at 120.0 °C in an oven for 24 h to remove surface-adsorbed water. The dried $CaCO_3$ (10 g) was ultrasonically suspended in 150 mL of ethyl acetate with ultrasonic stirring, and then 0.5 g KH-570 was added. The resulting suspension was transferred into a flask and stirred under reflux at 75 °C for 3.5 h. Upon completion of the reaction, the solid product was isolated via filtration, washed thoroughly three times with ethyl acetate, and finally subjected to vacuum drying at 50 °C for 24 h, yielding $HCaCO_3$ powders.

2.3. Synthesis of acrylic resin enhanced by hydrophobic calcium carbonate

Acrylic resin enhanced by hydrophobic calcium carbonate (ARH) was synthesized by emulsion polymerization. 30 g styrene and 10 g methyl methacrylate were thoroughly mixed using magnetic stirring for 15 min. Afterward, 10 g of $HCaCO_3$ was introduced into the previously prepared solution with vigorous stirring to achieve uniform dispersion. 10 g acrylamide and 15 g OS were then added to a 140 g water solution with ultrasonic dispersion for 15 min as the water phase. The aqueous phase was gradually introduced into the organic phase using a homogenizer at a speed of 3000 rpm for 10 min. The mixture was placed into a three-neck flask, followed by heating to a temperature of 80 °C, after which 0.075 g of ammonium persulfate (pre-dissolved in 2.5 mL distilled water) was introduced as an initiator. The mixture solution underwent reaction at 80 °C for 3.5 h to obtain a uniform acrylic resin emulsion enhanced by $HCaCO_3$ (ARH). The acrylic resin (AR) was synthesized using an identical method, except without the addition of $HCaCO_3$. For comparison, the acrylic resin with $CaCO_3$ (ARC) was prepared under the same conditions, incorporating unmodified $CaCO_3$ into the formulation. Fig. 1 displays the synthetic route of ARH. Initially, KH-570 is hydrolyzed and grafted onto the –OH of $CaCO_3$ particles, achieving hydrophobic surface modification (Fig. 1(a) and (b)). Subsequently, acrylamide, methyl methacrylate, and styrene monomers are polymerized on the $HCaCO_3$ via free-radical polymerization initiated by ammonium persulfate to obtain the ARH particles (Fig. 1(c)).

2.4. Characterization of acrylic resin enhanced by hydrophobic calcium carbonate

2.4.1. Structural and physicochemical properties

Fourier transform infrared spectroscopy (FT-IR) analysis was examined using IRTacer-100 (Shimadzu, Japan) to verify the molecular structure information of the synthesized products. X-ray diffraction patterns were collected by an X-ray diffractometer to obtain the crystal structure (PANalytical X-pert 3, Almelo, Netherlands). Solid-state NMR spectra were recorded on a Bruker-AVANCE 400 spectrometer with a resonance frequency of 400 MHz (^1H).

2.4.2. Thermodynamic analysis

The thermal decomposition characteristics of AR and ARH were investigated using a thermo-gravimetric analyzer (TA Instruments, USA). The heating program of this experiment was set from 30 to 600 °C at a constant heating rate of 10 °C per minute.

The glass transition temperature (Tg) is one of the key properties of polymers. A differential scanning calorimeter (DSC, NETZSCH, Germany) is used to confirm the Tg of AR and ARH. Under a nitrogen atmosphere, the sample was heated progressively from ambient conditions to 300 °C, applying a heating rate of 5 °C/min.

2.5. Performance evaluation tests of drilling fluid

2.5.1. Rheology and filtration loss experiments

To prepare the base fluid, 400 g of sodium bentonite (Na-Bent) and 14 g of Na_2CO_3 were incrementally added into 10,000 mL of deionized water under vigorous agitation for 24 h to complete hydration and form a 4% bentonite base fluid. Subsequently, different weight-to-volume ratios of AR and ARH were introduced into 400 mL portions of the prepared base fluid. The mixtures were subsequently homogenized at 6000 rpm, with the process maintained for 20 min to ensure uniform dispersion of the additives.

Each drilling fluid formulation was thermally treated in a roller oven at 180 °C over a period of 16 h to evaluate its thermal aging characteristics. Both rheological performance and filtration loss were evaluated following the procedures outlined by the American

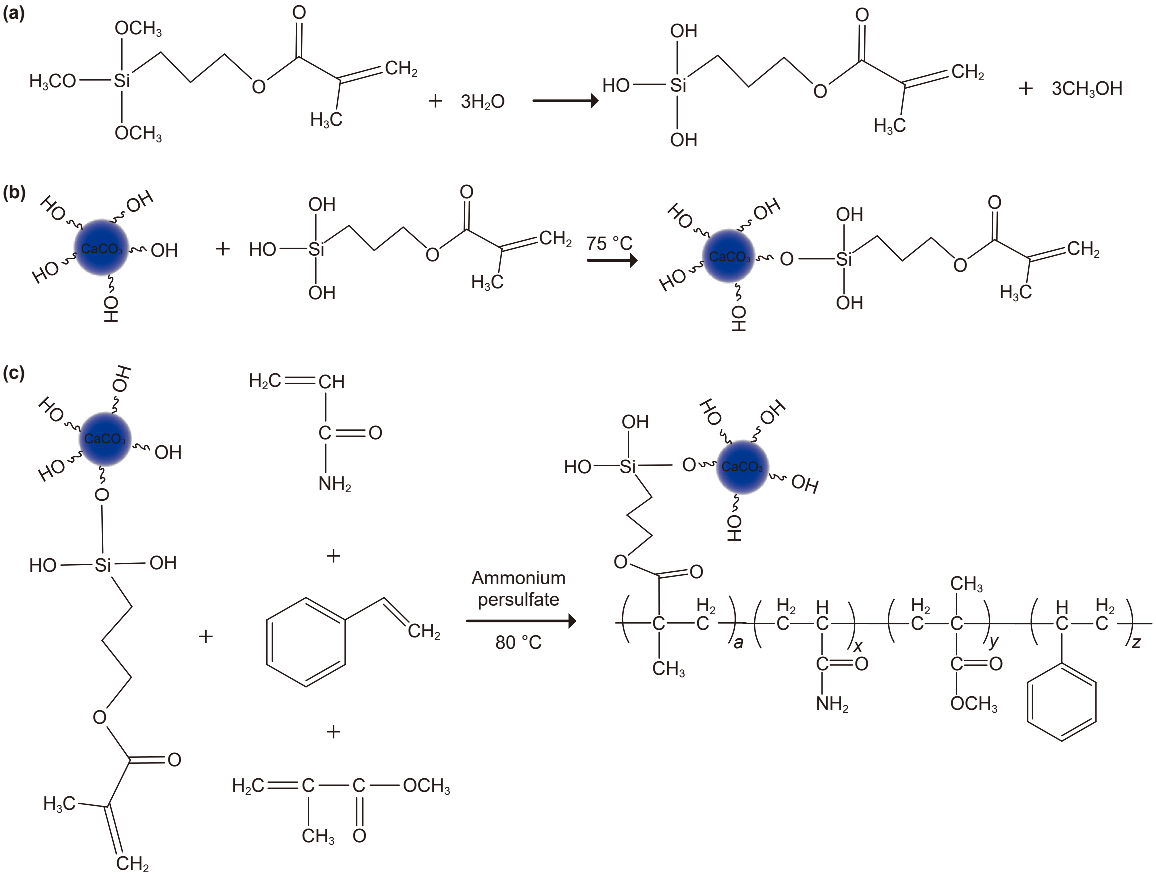

Fig. 1. Synthesis of acrylic resin enhanced by $HCaCO_3$ (ARH).

Petroleum Institute (API). Apparent viscosity (AV), plastic viscosity (PV), and yield point (YP) were calculated based on dial readings recorded at 600 and 300 rpm (θ_{600} and θ_{300}), using the standard API formulae:

$$AV = \theta_{600}/2\ (\mathrm{mPa{\cdot}s}) \tag{1}$$

$$PV = \theta_{600} - \theta_{300}\ (\mathrm{mPa{\cdot}s}) \tag{2}$$

$$YP = (\theta_{300} - PV)/2\ (\mathrm{Pa}) \tag{3}$$

Filtration loss experiments were performed using a medium-pressure filtration apparatus (SD4) manufactured by Qingdao Haitongda Special Instrument Co., Ltd. A filter paper featuring pore sizes ranging from 2 to 5 μm was used as the filtration medium. The cumulative volume of filtrate was recorded after 30 min of operation under a constant pressure of 0.7 MPa.

2.5.2. *Wellbore strengthening performance*

Lap shear strength tests were conducted on a universal testing machine (WDW-200, Shanghai Precision Instrument Co., Ltd.) to examine the anti-shear performance. In a lap shear test, the core samples were cut into rectangular slices measuring 3 cm by 15 cm, with a bonding area of 3 cm by 10 cm. Using a spoon equipped with a spatula at one end, 2 g AR or ARH were uniformly spread onto one core slice. Another core slice was then placed on top to fully cover the coated surface. The two slices were secured together using a clamp and then transferred to an oven at 160 °C for 4 h. Next, the samples were permitted to cool to ambient conditions, followed by the removal of the clamp and the measurement of shear strength. Test speed is set at 5 mm per minute. Shear strength is calculated by dividing the maximum shear force by the corresponding contact area.

Compressive strength tests were carried out on the same universal testing machine. Three artificial cores were made using the following method. First, 50 g of 40–80 mesh rock cuttings were mixed with 14 g of aqueous solution containing the sample at a 50% mass fraction, and the mixture was stirred thoroughly to ensure uniformity. Then, the rock cuttings with sample aqueous solutions were loaded into a core pressing mold and compressed with a pressure of 5 MPa to obtain complete rock columns. Next, the rock columns were heated in an oven maintained at 160 °C for 4 h. The compressive strength tests were conducted after the core column had cooled at room temperature. To investigate the impact of ARH on the strength of formation cores, standard shale core columns from the same block were soaked in aqueous solution and base fluid (with an ARH concentration of 2%) for 12 h, then dried at 100 °C, after which unconfined compressive strength tests were conducted.

2.5.3. *Plugging performance*

Plugging performance was carried out in the medium pressure filtration apparatus using microporous membranes with varying pore dimensions (0.1, 0.2, and 0.45 μm) as the filtration media. The data on filtration loss with increasing time was collected using an electronic balance connected to a computer. After the plugging experiments, the dried microporous membranes were analyzed to determine shifts in pore size characteristics employing a membrane pore size analyzer (iPore 900, China).

3. Results and discussion

3.1. Characterization of physicochemical properties

Fig. 2 shows the FT-IR spectra of $CaCO_3$, $HCaCO_3$, AR, ARC, and ARH. The absorption bands at 871 and 710 cm^{-1} represent typical vibrations of calcium carbonate (Fu et al., 2023; Kristova et al., 2015). Absorption peaks at 2954, 2872, and 1160 cm^{-1} in $HCaCO_3$ can be assigned to the bending vibrations of $–CH_3$, $–CH_2$, and the stretching vibration of Si–O. It can be inferred that KH-570 modified $CaCO_3$ successfully (Li et al., 2015). The determination results about the activation degree of $HCaCO_3$ in the supporting information also confirm this point. The absorption peaks of AR, ARC, and ARH around 1731 cm^{-1} are attributed to the stretching vibrations of the C=O functional group. The characteristic peak of $CaCO_3$ with 871 cm^{-1} appears in the curves of the ARC and ARH spectra (Tang et al., 2014; Yerro et al., 2016), indicating the incorporation of $CaCO_3$/$HCaCO_3$ in ARC/ARH. The absorption peak of the Si–O bond overlaps with the characteristic peaks of the polymer. Therefore, the Si–O peak was not discernible in the ARH sample (Cai et al., 2010).

As exhibited in Fig. 3, pristine $CaCO_3$, $HCaCO_3$, AR, ARC, and ARH are examined through XRD patterns to verify the crystalline structure and phase constituents. Diffraction peaks located at 2θ values of 23.1°, 29.5°, 36°, 39.5°, 43.1°, 47.6°, 48.6°, 56.4°, and 57.5° correspond to the crystallographic planes (012), (104), (110), (113), (202), (018), (116), (211), and (122), which are characteristic of the calcite form of $CaCO_3$ (Li et al., 2010). $HCaCO_3$ possesses the same peaks as the calcite structure, indicating that hydrophobic modification has no significant effect on the crystal form of calcium carbonate. The XRD pattern of AR shows no obvious diffraction peaks, possibly because the polymer chains exist in a disordered state without regular crystalline structures. The peaks of the ARH sample in the XRD pattern appear in the same positions but with lower intensity, compared with $CaCO_3$ and $HCaCO_3$, which can be attributed to the adsorption of the amino group in ARH on the crystal plane and inhibits its further growth (Li et al., 2010; Wang et al., 2006; Lakshminarayanan et al., 2003; Mahadevan et al., 2021). It is generally believed that inorganic materials exhibit poor compatibility with polymers (Kickelbick, 2003; Althues et al., 2007). As observed in Fig. S1, due to the poor compatibility between calcium carbonate and the polymer matrix in the ARC sample, unmodified calcium carbonate particles agglomerate during the emulsion polymerization process, forming large-sized aggregated particles. Therefore, the subsequent structural and performance characterizations are not pursued in this study.

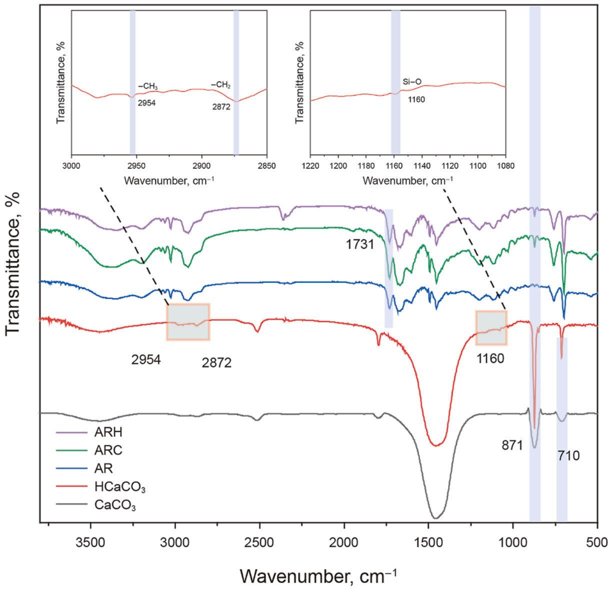

Fig. 2. FT-IR spectra of different samples.

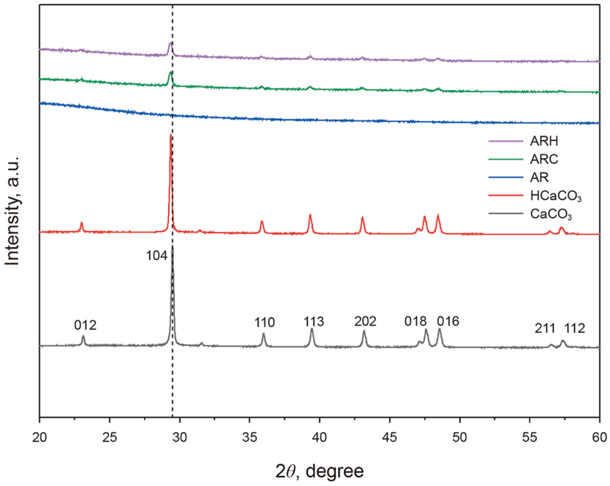

Fig. 3. XRD spectra of different samples.

Solid-state NMR spectra provide the structural information of insoluble composite materials. As shown in Fig. 4(a), the chemical shift at 5.5 ppm resonance originates from olefinic protons. The broad signals at 6.4 and 6.0 ppm are associated with –OH groups, and the 4.1 ppm peak is due to methine/methylene protons adjacent to a carbonyl. In addition, the 1.8 and 1.3 ppm resonances correspond to Si–CH_2 protons from KH-570. Consistency with literature chemical-shift ranges substantiates the conclusion that KH-570 is grafted onto calcium carbonate (National Institute of Industrial Science and Technology). As for AR in Fig. 4(b), the aromatic proton signal appeared at 6.8 ppm can be attributed to the benzene ring structure. The characteristic peak at 3.5 ppm corresponds to the methyl protons adjacent to the carbonyl group. As displayed in Fig. 4(c), the characteristic peak at 8.3 ppm is assigned to the amino proton (Ng et al., 2001). The aromatic protons exhibit characteristic signals at 7.2 and 6.5 ppm (Wegner et al., 2011). The peak at 3.1 ppm corresponds to the methyl protons adjacent to the carbonyl group (Chang et al., 2002). Meanwhile, the signal at 1.2 ppm originates from the methylene protons of the KH-570 component. The coexistence of the methylene signal of KH-570 at 1.2 ppm with characteristic resonance peaks of other monomers, such as aromatic proton peaks at 6.8, 7.2, and 6.5 ppm (from styrene monomer), the proton peak of the carbonyl group-adjacent methyl from methyl methacrylate monomer at 3.1 ppm, and the amino proton peak of acrylamide monomer at 8.3 ppm in the spectra confirms that the methacryloxy groups on the $CaCO_3$ surface have copolymerized with other vinyl monomers.

3.2. Thermodynamic performance analysis

As petroleum exploration and drilling operations increasingly target deeper and ultra-deep formations, there is a growing demand for drilling fluid additives possessing enhanced thermal stability. Therefore, the thermal stability of AR and ARH is investigated by TGA. As presented in Fig. 5(a) and (b), the weight loss of AR and ARH can be categorized into three distinct phases. The first stage of weight loss for AR and ARH occurs at temperatures of 30–199.2 °C and 30–181.7 °C, respectively. This stage is assigned to

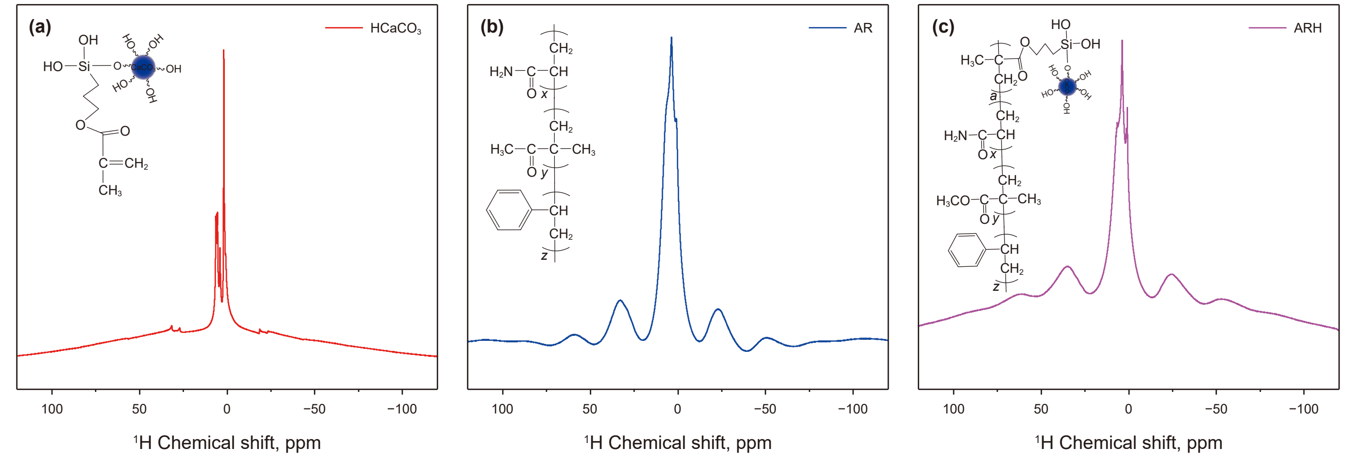

Fig. 4. Solid-state NMR spectra of $HCaCO_3$ (**a**), AR (**b**), and ARH (**c**).

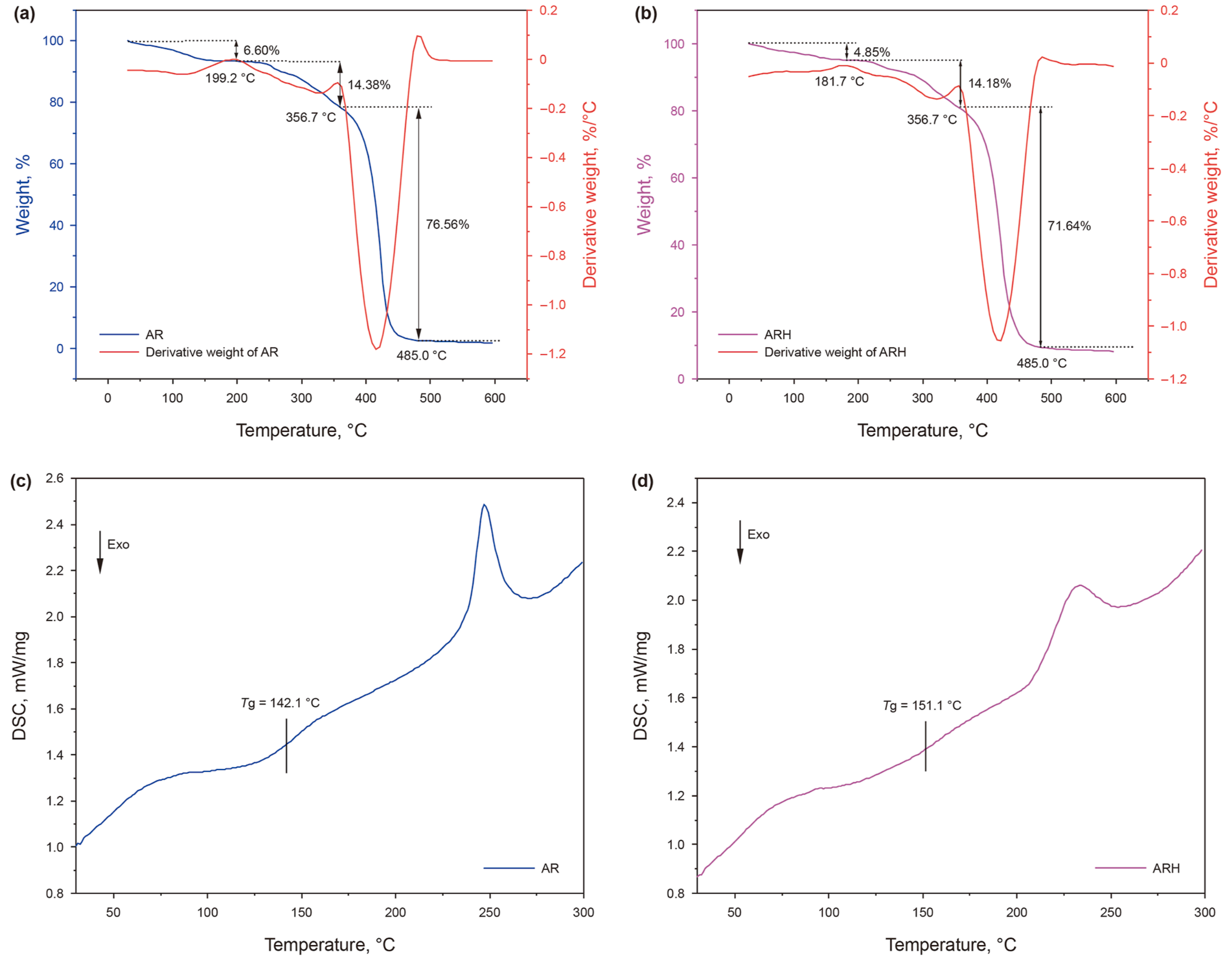

Fig. 5. TGA (**a**, **b**) and DSC (**c**, **d**) of AR and ARH.

the evaporation of free water and physically adsorbed water. The next decomposition stage ranges from 199.2 to 356.7 °C for AR and from 181.7 to 356.7 °C for ARH, with weight losses of 14.38% and 14.18%, respectively, mainly attributed to the degradation of a small portion of side chains. The third stage ranges from 356.7 to 485 °C, with total weight losses reaching 97.45% for AR and 90.8% for ARH. The final residue of ARH was 6.87% greater by weight compared to AR, which can be attributed to the calcium carbonate encapsulated by the acrylic resin.

DSC curves of AR and ARH are shown in Fig. 5(c) and (d). The glass transition temperatures (*Tg*) of AR and ARH are 142.1 and 151.1 °C, respectively, indicating that incorporating $HCaCO_3$

improves the *Tg* of the samples. The increased *Tg* value of ARH may result from interactions formed between $HCaCO_3$ and the acrylic resin, which restricts polymer chain movement and then elevates the *Tg* value (Zhang et al., 2024; Lu and Nutt, 2003). Previous studies have verified that attractive particle-polymer interaction may cause slower dynamics of polymers and lead to increased *Tg* values (Klonos et al., 2016; García-Chávez et al., 2013).

3.3. Morphology of AR and ARH

Fig. 6 displays the morphology of AR and ARH. AR exhibits uniform spheres with an approximate *Z*-average diameter of 72 nm (Fig. 6(a–c)). When enhanced by $HCaCO_3$, it can be observed that the light gray polymer shell coats the inorganic $HCaCO_3$ particles in Fig. 6(b), and the *Z*-average diameter increases to 277.6 nm from Fig. 6(c). The apparent photographs of AR and ARH can distinguish the difference between AR and ARH (Fig. 6(d)). AR is transparent with a bluish hue and exhibits good fluidity. After the addition of $HCaCO_3$, the resulting ARH becomes milky white with increased particle size, which further demonstrates that $HCaCO_3$ is successfully incorporated into the ARH, causing changes in appearance, particle size, and flow behavior.

3.4. Rheology and filtration loss performance

The key indicators that govern the operational safety and effectiveness of drilling fluids are their rheological behavior and fluid loss control capability. Thus, the rheological properties and filtration behavior of AR and ARH in base fluid are examined in Fig. 7. As for AV in Fig. 7(a), the values exhibit a mild rise from 10.5 to 12 mPa·s with the increased concentrations from 0.5% to 2% before aging. After undergoing heat treatment at 180 °C for 16 h, the AV of the base fluid with 2% ARH increases to 12.5 mPa·s as a result of ARH interacting with clay particles, thus enhancing the grid structure of the drilling fluid. The same trend also appears in PV changes in Fig. 7(b). For example, the PV value of the base fluid with 2% ARH increases by 3 mPa·s in comparison to the PV value of the base fluid. As presented in Fig. 7(c), adding ARH may slightly affect the YP value. For filtration performance in Fig. 7(d), incorporating ARH displays minimal influence on fluid loss before aging. Nevertheless, following thermal aging at 180 °C for 16 h, the

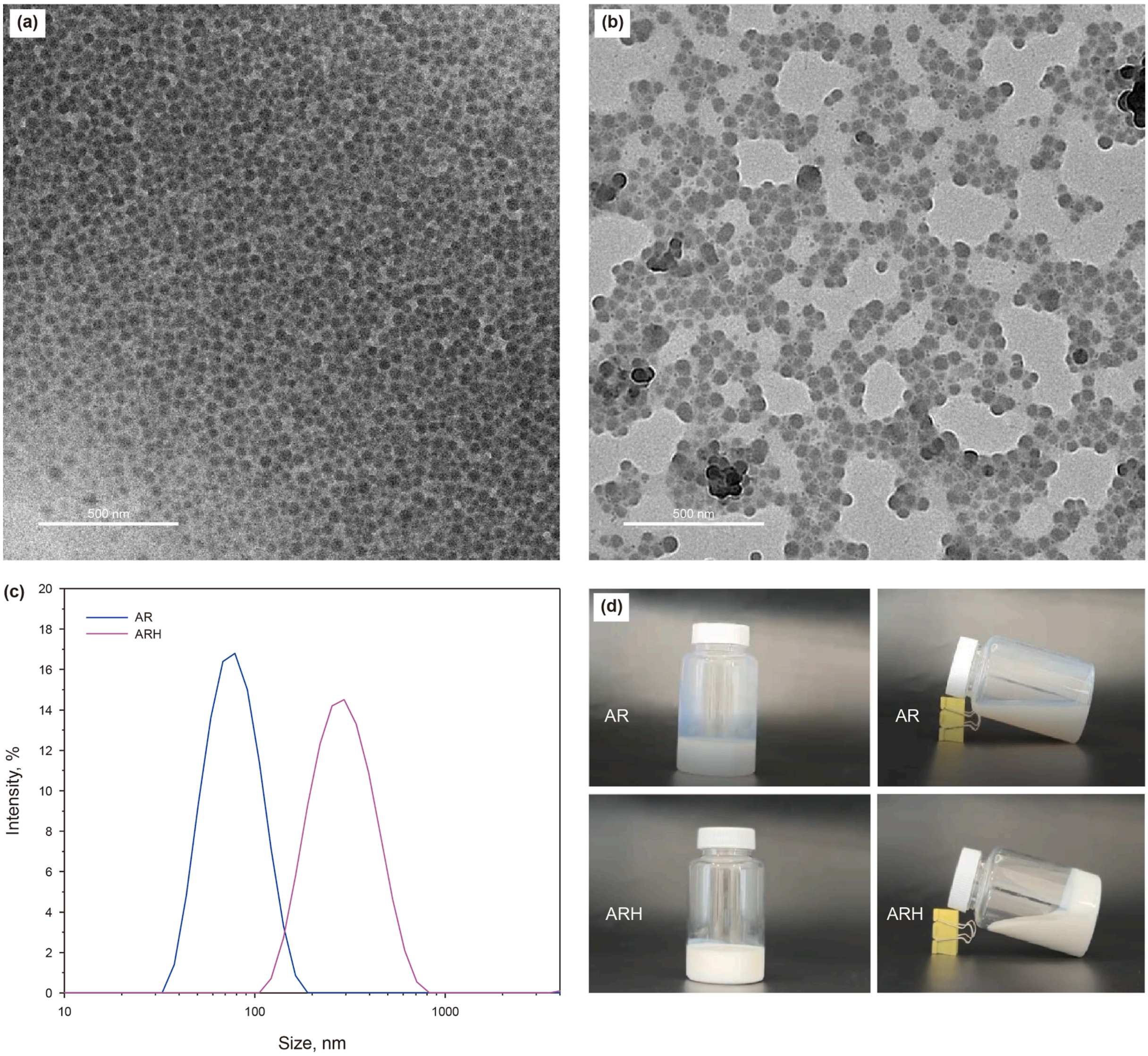

Fig. 6. TEM images (**a**, **b**), particle size distribution (**c**), and photographs (**d**) of AR and ARH.

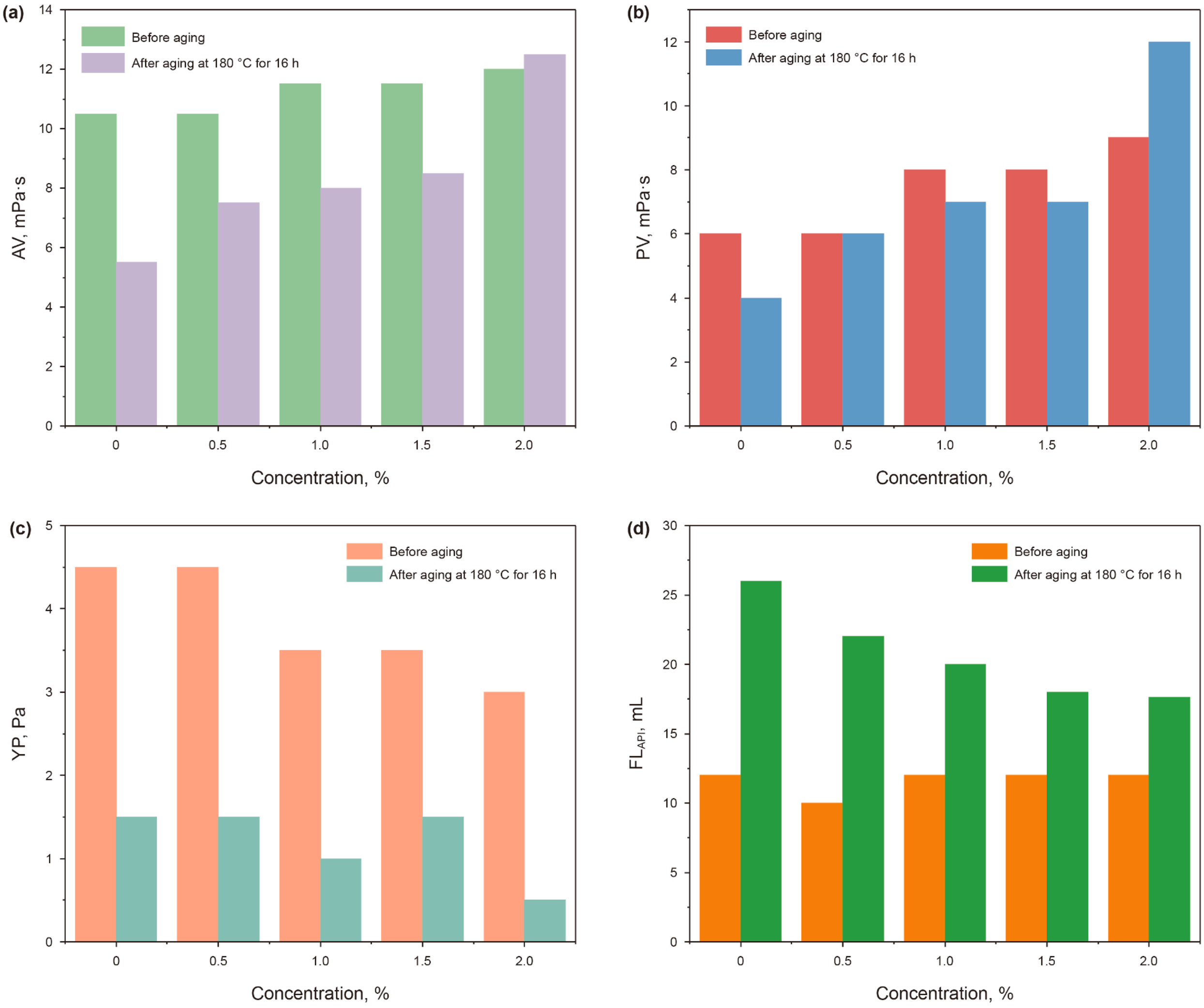

Fig. 7. Rheological (**a**, **b**, **c**) and filtration performance (**d**) of base fluid before and after aging at 180 °C for 16 h with increasing concentration of ARH.

base fluid exhibits a noticeable reduction in fluid loss upon the incorporation of varying concentrations of ARH. At an ARH concentration of 2%, the fluid loss reaches 17.6 mL, representing a reduction of 8.4 mL compared to the aged base fluid without ARH. Overall, the addition of ARH in the base fluid shows little effect on AV, PV, and YP, but it effectively reduces fluid loss.

3.5. *Wellbore strengthening performance*

3.5.1. *Lap shear strength test*

The lap shear strength test can effectively reflect the adhesive performance of additives in drilling fluid. Fig. 8(a) illustrates the schematic of the lap shear strength test, where AR or ARH is utilized to adhere core slices under vertical tension forces. Fig. 8(b) and (c) present the appearance of core slices bonded by AR and ARH before and after the lap shear strength test. Fig. 8(d) shows the relationship between displacement and stress using AR and ARH to adhere core slices. As displacement increases, the stresses rise to peaks and then drop sharply. As for AR, the shear strength is determined to be 0.1311 MPa, whereas the shear strength of the ARH reaches 0.4838 MPa, representing a significant improvement compared to the AR, with an improvement of 0.3527 MPa. This result demonstrates that the addition of inorganic materials notably enhances adhesive performance, which is of great importance for fractured formations with poor adhesion properties.

3.5.2. *Compressive strength test*

To simulate the fractured formation, artificial standard core columns (2.5 cm × 5.0 cm) were made with 40–80 mesh rock cuttings. The photographs of three artificial core columns before and after the compressive strength test are presented in Fig. 9(a–f). It is noticed that the stresses of all samples rise to peaks with increased displacement, and then drop to zero (Fig. 9(g)). Although water treatment alone can produce core columns with an intact appearance, they display pronounced deformation and fracturing under low stress. The AR shows moderate improvement, with a maximum stress of 2.2118 MPa. Notably, the ARH demonstrates superior mechanical performance, with a peak stress of 7.1567 MPa and the most significant displacement before failure, indicating enhanced strength and toughness. The findings indicate that the introduction of $HCaCO_3$ greatly enhances interfacial compatibility with the polymer matrix, leading to improved mechanical performance of the ARH sample.

To more precisely reflect the effect of ARH on the compressive strength of shale cores, uniaxial compressive strength tests were conducted after immersing the shale core samples in different fluid systems. Shale core columns before and after compressive

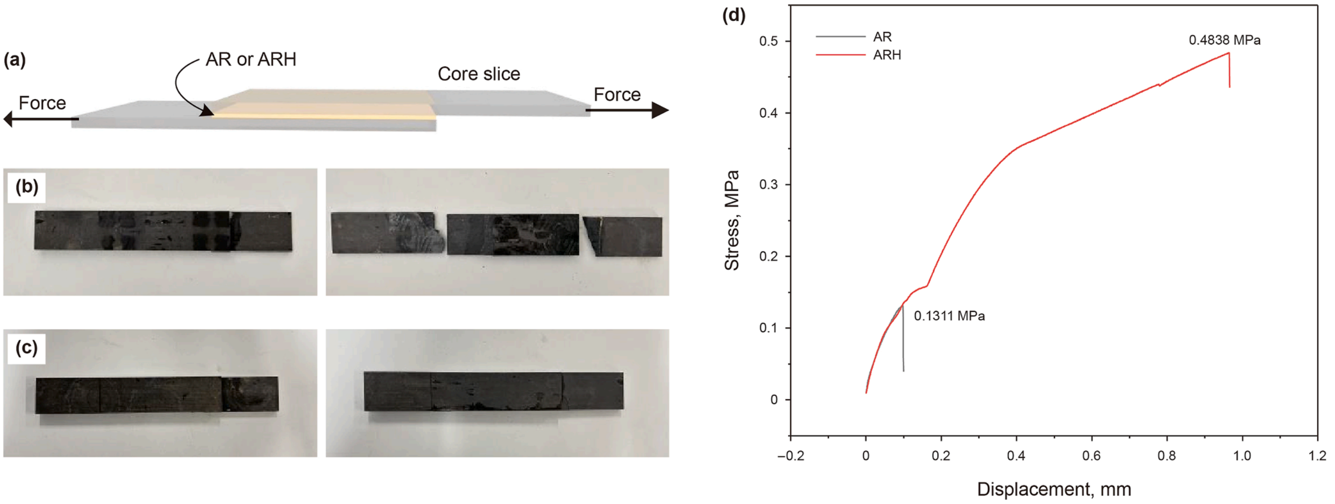

Fig. 8. Schematic diagram of lap shear strength test (**a**), sample images of core slices adhered by AR (**b**) and ARH (**c**) before and after lap shear strength test, and curves of stress-displacement (**d**).

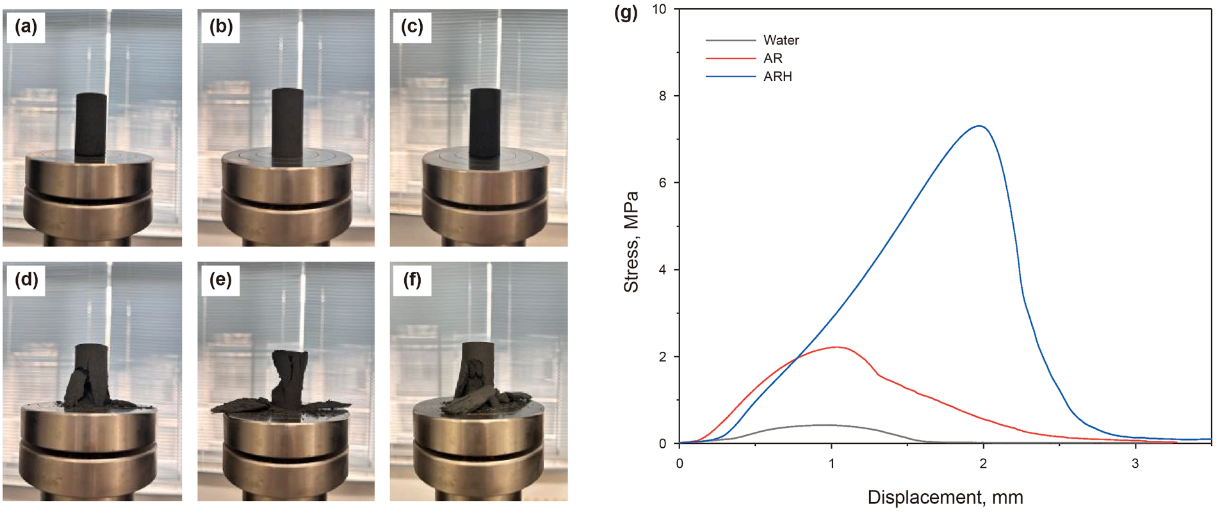

Fig. 9. Photographs of rock core columns before (**a**, **b**, **c**) and after (**d**, **e**, **f**) compressive strength tests and stress-displacement curves of rock cores (**g**) treated with different samples.

strength tests are displayed in Fig. S2. As shown in Fig. 10(a), the peak compressive strength of the core soaked in water is 63.1075 MPa, whereas immersion in the ARH aqueous solution increases the stress to 81.1695 MPa. Compared to the base fluid alone (with a compressive strength of 50.7299 MPa), Fig. 10(b) further demonstrates that the addition of ARH to the base fluid markedly enhanced the core strength to 69.6446 MPa. The results further indicate that incorporating ARH can conspicuously improve the mechanical strength of rock cores.

3.6. *Plugging performance*

Plugging formation pores and fractures serves as a practical approach for preventing drilling fluid penetration into reservoir rock and maintaining borehole integrity. Hence, plugging experiments were conducted using microporous filter membranes of 0.1, 0.2, and 0.45 μm as filtering substrates to evaluate the plugging effect on small-pore formations. As shown in Fig. 11(a–c), the filtration loss of solution through microporous filter membranes increases sharply at first and gradually turns to be steadied. Fluid loss declines with the rising concentration of ARH. When the concentration increases to 2%, the filtration losses through microporous filter membranes of 0.1, 0.2, and 0.45 μm were decreased to 13.5, 13.2, and 27 mL, respectively, indicating excellent plugging performance for nanopores. For the 0.2 μm microporous membrane, the increased particles (*Z*-average diameter is 277.6 nm) are slightly larger than the pore size, allowing them to quickly form a robust and dense bridging structure at the pore entrance. This optimal particle-to-pore size ratio enables the ARH particles to rapidly establish a dense and stable filter-cake bridging layer at the pore throat. Such a suitable size match ensures that the particles neither penetrate deeply into the pore structure, causing loose blockage, nor are too large to effectively accumulate, thus efficiently preventing fluid infiltration and significantly reducing filtration loss. This ideal match between particle size and pore size demonstrates the core principle of the particle bridging plugging theory, effectively explaining the lowest filtration loss observed with the 0.2 μm membrane.

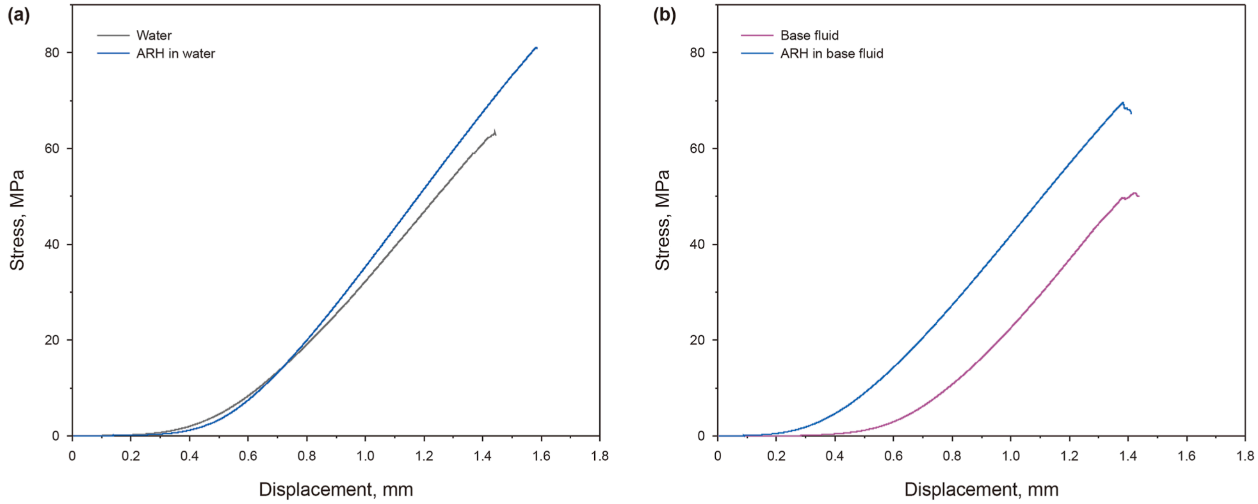

Fig. 10. Stress-displacement curves of shale core samples treated with water, ARH aqueous solution (**a**), base fluid, and ARH (**b**) in base fluid.

The changes in pore size distribution after plugging with ARH are shown in Fig. 11(d–f). Initially, the membrane pore sizes are concentrated around 100 nm (Fig. 11(d)). With increasing ARH concentrations (0.5%, 1.0%, 1.5%, and 2.0%), the pore size distribution shifts toward smaller diameters, indicating that larger pores are effectively blocked. However, due to the relatively small pore size, larger particles struggle to fully penetrate and plug the pores, leaving some larger pores inadequately plugged. As exhibited in Fig. 11(e), for the 0.2 μm membrane, after treatment with varying concentrations of ARH, a noticeable refinement in pore size distribution occurs, particularly at higher concentrations (1.5% and 2.0%), where larger pores virtually disappear. This indicates that the particle size is ideally matched to the 0.2 μm pores, rapidly and efficiently forming a dense and stable bridging layer at the pore entrances, resulting in superior plugging performance. After ARH plugs the 0.45 μm membrane, the pore size distribution slightly decreases, and larger pores remain incompletely plugged, indicating that the particles are relatively small compared to the pore size, resulting in limited plugging efficiency (Fig. 11(f)).

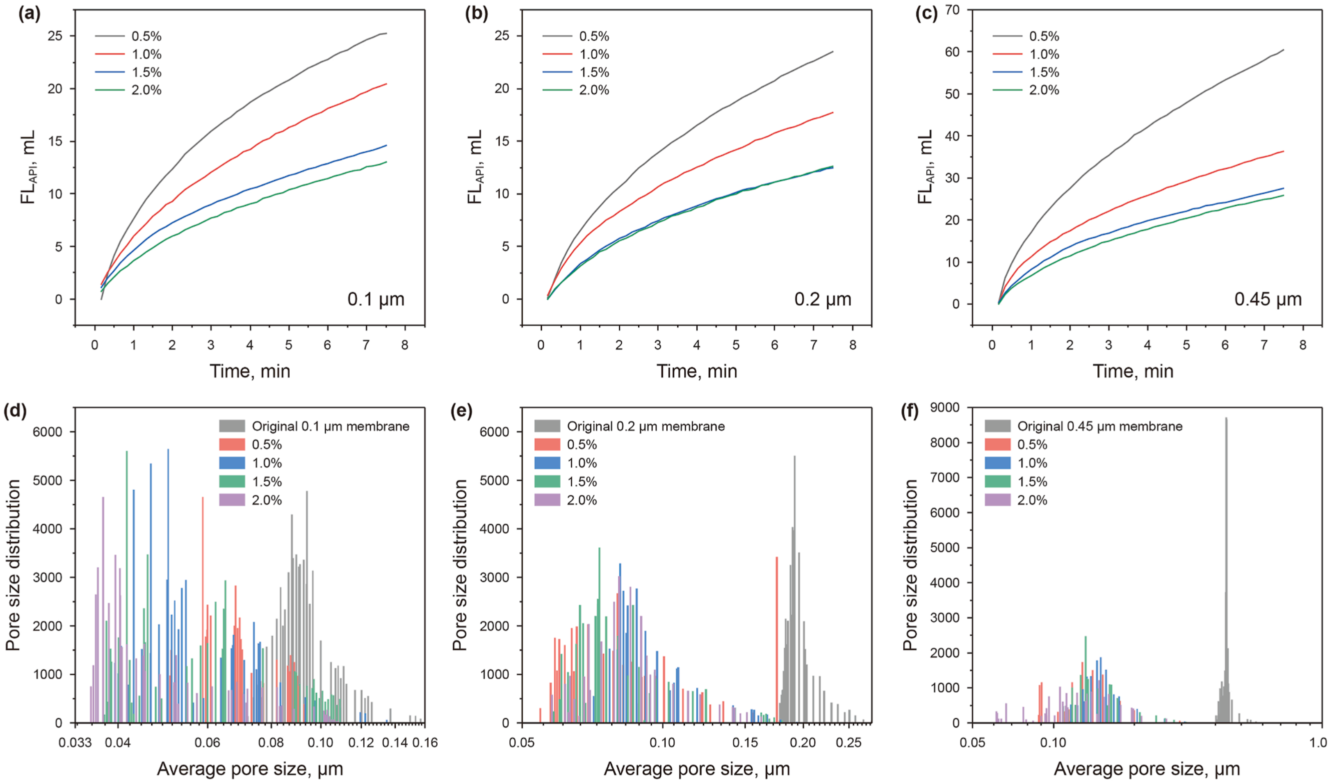

Fig. 11. The variation of fluid loss over time after plugging with microporous filter membranes of different pore sizes (**a**, **b**, **c**) and pore size distribution of the membrane before and after plugging (**d**, **e**, **f**).

3.7. *Wellbore strengthening mechanism*

As shown in Fig. 12(a), the developed wellbore strengthening material (ARH) achieves effective plugging and cementation of pores and fractures in fractured formations through the synergistic interaction between the two core components: polymeric matrix and hydrophobically modified calcium carbonate particles ($HCaCO_3$). The combined action forms a robust plugging and rock-bonding effect at the wellbore wall, thereby strengthening the wellbore.

Specifically, the $HCaCO_3$ particles in ARH first form a rigid supporting framework through physical accumulation and fracture filling. Meanwhile, the polymeric matrix in ARH enhances wellbore stability through interactions with the fractured formation. When the polar amide groups in the polymer molecular chains come into contact with the formation rock surface, they form strong intermolecular hydrogen bonds and van der Waals forces, significantly improving the adhesive force between ARH and the rock. Simultaneously, the polymer chains exhibit strong cohesive force via hydrogen bonding, π-π stacking, and physical entanglement, ensuring that the polymer structure is not easily damaged, which would lead to bonding failure (Zhang et al., 2025; Xiao et al., 2022; Kou et al., 2025).

As depicted in Fig. 12(b), fractured formations are prone to instability during drilling operations (manifested as rock fragment detachment or borehole collapse), and such issues are further exacerbated by the infiltration of drilling fluid (Wang et al., 2020; You et al., 2014). When ARH is added to WBDF, it efficiently penetrates the microscopic pores and fractures of the formation with fluid flow. As the downhole temperature gradually exceeds the glass transition temperature (*Tg*) of the polymeric matrix, the polymer molecular segments gain mobility, causing the matrix to soften and undergo elastic deformation (Kumar et al., 2023; Hameed et al., 2007). This elastic behavior allows the polymer to conform to the irregular geometry of pores and fractures, while the $HCaCO_3$ particles provide the support within this elastic structure. Through their synergistic spatial complementarity, tight and comprehensive filling is achieved, significantly enhancing wellbore stability.

4. Conclusions

This study develops a novel acrylic-based wellbore strengthening material (ARH) by incorporating hydrophobically modified calcium carbonate particles to mitigate wellbore instability under complex geological conditions. ARH exhibits uniform spherical particles characterized by a *Z*-average diameter of 277.6 nm. TGA and DSC analysis indicate ARH possesses excellent thermal stability, with an onset decomposition temperature exceeding 180 °C and a *Tg* value of 151.1 °C, indicating its suitability for applications under high-temperature conditions. Mechanical testing reveals excellent adhesion strength (0.4838 MPa) in lap shear strength tests and substantial core reinforcement, achieving a uniaxial compressive strength of 7.1567 MPa. Compared to shale core columns soaked in water and base fluid, the compressive strength of shale cores treated with ARH increased by 18.0620 and 18.9147 MPa, respectively. Microporous membrane plugging experiments further confirm ARH's superior plugging ability, with

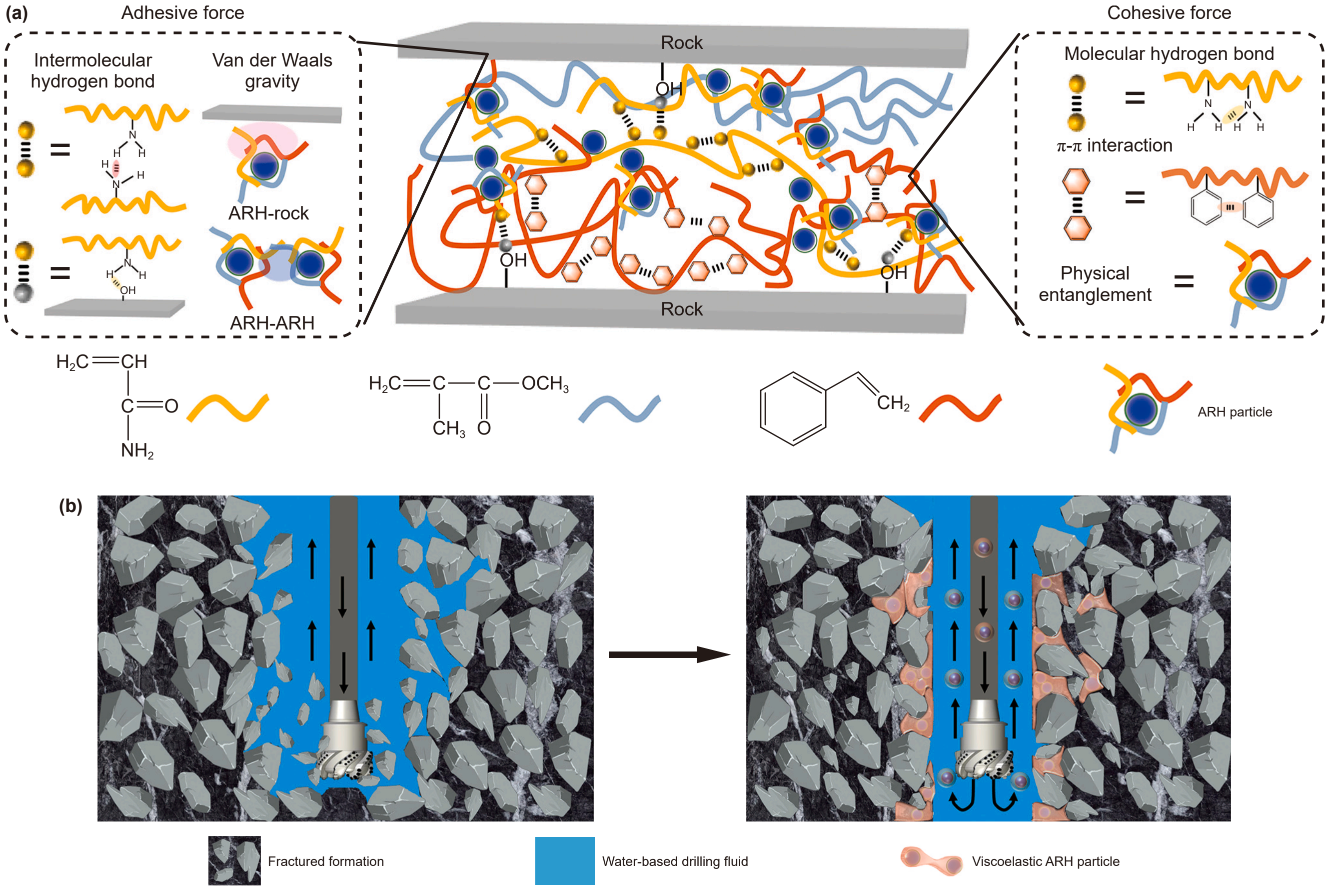

Fig. 12. Wellbore strengthening mechanism of ARH.

filtration loss volumes of 13.5, 13.2, and 27 mL through 0.1, 0.2, and 0.45 μm membranes, respectively, at an added ARH concentration of 2%. These results highlight ARH's excellent plugging and wellbore strengthening properties, making it a promising candidate for wellbore strengthening material in WBDF.

Although ARH has demonstrated excellent thermal resistance, mechanical strength, and plugging performance, there remains potential for further performance enhancement through material and process optimization. In particular, the grafting efficiency of KH-570 onto calcium carbonate plays a critical role in determining the dispersion stability and interfacial compatibility of the modified particles within the resin matrix. Future studies could explore the hydroxylation of $CaCO_3$ before KH-570 modification to increase the density of reactive –OH groups on the particle surface. This pretreatment is expected to facilitate a higher grafting rate, thereby enhancing the interfacial bonding and overall performance of the composite material. Additionally, investigations into alternative coupling agents, surface activation methods, and resin formulations may provide new insights into optimizing ARH for broader applications in extreme drilling environments.

In summary, this study developed a novel acrylic-based wellbore strengthening material by incorporating hydrophobically modified calcium carbonate into the acrylic resin matrix, providing a new material solution for enhancing wellbore stability in WBDF systems.

CRediT authorship contribution statement

Kai-He Lv: Visualization, Validation, Supervision, Resources, Project administration, Conceptualization. **Juan He:** Visualization, Investigation, Formal analysis, Data curation. **Xian-Bin Huang:** Resources, Methodology, Funding acquisition, Conceptualization. **Jin-Sheng Sun:** Visualization, Validation, Funding acquisition, Conceptualization.

Declaration of Competing Interests

The authors declare that they have no known competing financial interests or personal relationships that could have appeared to influence the work reported in this paper.

Acknowledgments

The study is supported by the Fundamental Research Funds for the Central Universities (No. 24CX02003A), the National Natural Science Foundation of China (52374024), and the Fund of State Key Laboratory of Deep Oil and Gas, China University of Petroleum (East China).

Appendix A. Supplementary data

Supplementary data to this article can be found online at https://doi.org/10.1016/j.petsci.2025.11.037.

References

Althues, H., Henle, J., Kaskel, S., 2007. Functional inorganic nanofillers for transparent polymers. Chem. Soc. Rev. 36 (9), 1454–1465. https://doi.org/10.1039/B608177K.

Cai, D.K., Neyer, A., Kuckuk, R., et al., 2010. Raman, mid-infrared, near-infrared and ultraviolet-visible spectroscopy of PDMS silicone rubber for characterization of polymer optical waveguide materials. J. Mol. Struct. 976 (1), 274–281. https://doi.org/10.1016/j.molstruc.2010.03.054.

Chang, L.L., Bruch, M.D., Griskowitz, N.J., et al., 2002. NMR spectroscopy for determination of cationic polymer concentrations. Water Res. 36 (9), 2255–2264. https://doi.org/10.1016/S0043-1354(01)00444-4.

Feng, Y.C., Gray, K.E., 2017. Review of fundamental studies on lost circulation and wellbore strengthening. J. Pet. Sci. Eng. 152, 511–522. https://doi.org/10.1016/j.petrol.2017.01.052.

Fu, J., Yap, J.X., Leo, C.P., et al., 2023. Carboxymethyl cellulose/sodium alginate beads incorporated with calcium carbonate nanoparticles and bentonite for phosphate recovery. Int. J. Biol. Macromol. 234, 123642. https://doi.org/10.1016/j.ijbiomac.2023.123642.

García-Chávez, K.I., Hernández-Escobar, C.A., Flores-Gallardo, S.G., et al., 2013. Morphology and thermal properties of clay/PMMA nanocomposites obtained by miniemulsion polymerization. Micron 49, 21–27. https://doi.org/10.1016/j.micron.2013.02.007.

Gu, S., Kondo, T., Konno, M., 2004. Preparation of silica-polystyrene core-shell particles up to micron sizes. J. Colloid Interface Sci. 272 (2), 314–320. https://doi.org/10.1016/j.jcis.2004.01.056.

Hameed, N., Sreekumar, P.A., Francis, B., et al., 2007. Morphology, dynamic mechanical and thermal studies on poly(styrene-co-acrylonitrile) modified epoxy resin/glass fibre composites. Compos. Part A: Appl. S. 38 (12), 2422–2432. https://doi.org/10.1016/j.compositesa.2007.08.009s.

He, Z., Yang, Y., Qi, J., et al., 2024. Hyperbranched polymer nanocomposite as a potential shale stabilizer in water-based drilling fluids for improving wellbore stability. J. Mol. Liq. 395, 123903. https://doi.org/10.1016/j.molliq.2023.123903.

Huang, X., Liu, F., Zhang, P., et al., 2023. Application of microgel latex in water-based drilling fluid to stabilize the fractured formation. Geoenergy Sci. Eng. 228, 212016. https://doi.org/10.1016/j.geoen.2023.212016.

Huang, X.B., Meng, X., Lv, K.H., et al., 2022. Development of a high temperature resistant nano-plugging agent and the plugging performance of multi-scale micropores. Colloids Surf. 639, 128275. https://doi.org/10.1016/j.colsurfa.2022.128275.

Jiang, H., Yang, H., Ning, C., et al., 2025. Amphiphilic polymer with ultra-high salt resistance and emulsification for enhanced oil recovery in heavy oil cold recovery production. Geoenergy Sci. Eng. 252, 213920. https://doi.org/10.1016/j.geoen.2025.213920.

Kickelbick, G., 2003. Concepts for the incorporation of inorganic building blocks into organic polymers on a nanoscale. Prog. Polym. Sci. 28 (1), 83–114. https://doi.org/10.1016/S0079-6700(02)00019-9.

Klonos, P., Kulyk, K., Borysenko, M.V., et al., 2016. Effects of molecular weight below the entanglement threshold on interfacial nanoparticles/polymer dynamics. Macromolecules 49 (24), 9457–9473. https://pubs.acs.org/doi/10.1021/acs.macromol.6b01931.

Kou, Z., Sha, Y., Liu, M., et al., 2025. Bio-based and recyclable adhesives based on β-hydroxyester bonds and hydrogen bonds via molecular dynamics simulation. J. Mater. Chem. A 13 (7), 5119–5129. https://doi.org/10.1039/D4TA06980C.

Kristova, P., Hopkinson, L.J., Rutt, K.J., 2015. The effect of the particle size on the fundamental vibrations of the $[CO_3^{2-}]$ anion in calcite. J. Phys. Chem. A 119 (20), 4891–4897. https://doi.org/10.1021/acs.jpca.5b02942.

Kumar, P.S., Jayanarayanan, K., Balachandran, M., 2023. High-performance thermoplastic polyaryletherketone/carbon fiber composites: Comparison of plasma, carbon nanotubes/graphene nano-anchoring, surface oxidation techniques for enhanced interface adhesion and properties. Compos. Part B-Eng. 253, 110560. https://doi.org/10.1016/j.compositesb.2023.110560.

Lakshminarayanan, R., Valiyaveettil, S., Loy, G.L., 2003. Selective nucleation of calcium carbonate polymorphs: Role of surface functionalization and poly(-vinyl alcohol) additive. Cryst. Growth Des. 3 (6), 953–958. https://doi.org/10.1021/cg034022j.

Lei, M., Huang, W.A., Sun, J.S., et al., 2022. The utilization of self-crosslinkable nanoparticles as high-temperature plugging agent in water-based drilling fluid. SPE J. 27 (5), 2628–2641. https://doi.org/10.2118/209805-PA.

Li, Y., Zhao, Z.F., Lau, Y.T.R., et al., 2010. Preparation and characterization of coverage-controlled $CaCO_3$ nanoparticles. J. Colloid Interface Sci. 345 (2), 168–173. https://doi.org/10.1016/j.jcis.2010.01.080.

Li, Y.L., Cai, J.G., Song, G.Q., et al., 2015. DRIFT spectroscopic study of diagenetic organic-clay interactions in argillaceous source rocks. Spectrochim. Acta, Part A 148, 138–145. https://doi.org/10.1016/j.saa.2015.03.131.

Liu, K.C., Wang, R., Rong, K.S., et al., 2023. Synthesis and plugging performance of nano-micron polymeric gel microsphere plugging agents for oil-based drilling fluids. Gels 9 (4), 290. https://www.mdpi.com/2310-2861/9/4/290.

Liu, S.X., Ott, W.K., 2020. Sodium silicate applications in oil, gas & geothermal well operations. J. Pet. Sci. Eng. 195, 107693. https://doi.org/10.1016/j.petrol.2020.107693.

Liu, X., Xiao, Y., Ding, Y., 2025. Research progress and prospects of nano plugging agents for shale water-based drilling fluids. ACS Omega 10 (6), 5138–5147. https://doi.org/10.1021/acsomega.4c07942.

Lu, H.B., Nutt, S., 2003. Restricted relaxation in polymer nanocomposites near the glass transition. Macromolecules 36 (11), 4010–4016. https://doi.org/10.1021/ma034049b.

Luo, Y., Shang, Q., Hu, H., et al., 2025. Preparation of expandable polymer plugging agent and its application in water-based drilling fluid. J. Appl. Polym. Sci. 142 (10), e56546. https://doi.org/10.1002/app.56546.

Mahadevan, G., Ruifan, Q., Hian, Jane Y.H., et al., 2021. Effect of polymer nano- and microparticles on calcium carbonate crystallization. ACS Omega 6 (31), 20522–20529. https://doi.org/10.1021/acsomega.1c02564.

National Institute of Advanced Industrial Science and Technology, 2021. Spectral Database for Organic Compounds (SDBS). SDBS No: 6845. https://sdbs.db.aist.go.jp/disclaimer.aspx.

Ng, C.C., Cheng, Y.L., Pennefather, P.S., 2001. One-step synthesis of a fluorescent phospholipid-hydrogel conjugate for driving self-assembly of supported lipid membranes. Macromolecules 34 (17), 5759–5765. https://pubs.acs.org/doi/10.1021/ma0100899.

Sun, J., Li, Y., Liao, B., et al., 2024a. Development and performance evaluation of bioenzyme-responsive temporary plugging materials. Adv. Geo-Energy Res. 11 (1), 20–28. https://www.yandy-ager.com/index.php/ager/article/view/1002.

Sun, J.S., Yang, J.B., Bai, Y.R., et al., 2024b. Research progress and development of deep and ultra-deep drilling fluid technology. Petrol. Explor. Dev. 51 (4), 1022–1034. https://doi.org/10.1016/S1876-3804(24)60522-7.

Tang, Z., Cheng, G., Chen, Y., et al., 2014. Characteristics evaluation of calcium carbonate particles modified by surface functionalization. Adv. Powder Technol. 25 (5), 1618–1623. https://doi.org/10.1016/j.apt.2014.05.017.

Tang, Z.C., Qiu, Z.S., Zhong, H.Y., et al., 2022. Wellbore stability through novel catechol-chitosan biopolymer encapsulator-based drilling mud. Gels 8 (5), 307. https://doi.org/10.3390/gels8050307.

Wang, B., Sun, J.S., Shen, F., et al., 2020. Mechanism of wellbore instability in continental shale gas horizontal sections and its water-based drilling fluid countermeasures. Nat. Gas. Ind. B 7 (6), 680–688. https://doi.org/10.1016/j.ngib.2020.04.008.

Wang, C.Y., Zhao, J.Z., Zhao, X., et al., 2006. Synthesis of nanosized calcium carbonate (aragonite) via a polyacrylamide inducing process. Powder Technol. 163 (3), 134–138. https://doi.org/10.1016/j.powtec.2005.12.019.

Wang, Q., Cai, J., Wang, J., et al., 2024. Development and application of the anti-high-temperature delayed crosslinking polymer as a gel plugging additive for drilling fluid. Gels 10 (1), 73. https://www.mdpi.com/2310-2861/10/1/73.

Wang, X., Jiang, G., Wang, G., et al., 2023. Application of a biomimetic wellbore stabilizer with strong adhesion performance for hydrate reservoir exploitation. Fuel 337, 127184. https://doi.org/10.1016/j.fuel.2022.127184.

Wegner, M., Dudenko, D., Sebastiani, D., et al., 2011. The impact of the amide connectivity on the assembly and dynamics of benzene-1,3,5-tricarboxamides in the solid state. Chem. Sci. 2 (10), 2040–2049. https://doi.org/10.1039/C1SC00280E.

Xiao, Z., Li, Q., Liu, H., et al., 2022. Adhesion mechanism and application progress of hydrogels. Eur. Polym. J. 173, 111277. https://doi.org/10.1016/j.eurpolymj.2022.111277.

Xu, Z., Sun, J.S., Li, L., et al., 2023. Development and performance evaluation of a high temperature resistant, internal rigid, and external flexible plugging agent for water-based drilling fluids. Petroleum 9 (1), 33–40. https://doi.org/10.1016/j.petlm.2022.07.004.

Yang, H., Jiang, H., Liu, T., et al., 2025a. Viscoelastic displacement mechanism of fluorescent polymer microspheres based on macroscopic and microscopic displacement experiments. Phys. Fluids 37 (4), 042022. https://doi.org/10.1063/5.0268850.

Yang, H.B., Jiang, H.Z., Xu, Z., et al., 2025b. Development and evaluation of organic/metal ion double crosslinking polymer gel for anti-CO_2 gas channeling in high temperature and low permeability reservoirs. Pet. Sci. 22 (2), 724–738. https://doi.org/10.1016/j.petsci.2024.11.016.

Yang, J.B., Bai, Y.R., Sun, J.S., et al., 2024. High-temperature, salt-resistant, and high-strength-controlled consolidated resin slurry for fracture plugging during oil and gas well drilling. SPE J. 29 (9), 4619–4632. https://doi.org/10.2118/221473-PA.

Yerro, O., Radojevic, V., Radovic, I., et al., 2016. Thermoplastic acrylic resin with self-healing properties. Polym. Eng. Sci. 56 (3), 251–257. https://doi.org/10.1002/pen.24244.

You, L., Kang, Y., Chen, Z., et al., 2014. Wellbore instability in shale gas Wells drilled by oil-based fluids. Int. J. Rock Mech. Min. 72, 294–299. https://doi.org/10.1016/j.ijrmms.2014.08.017.

Zhang, S.W., Wang, R., Zhang, J.L., et al., 2025. Enhancing dispersion and mechanical properties of carbon nanotube-reinforced cement-based material using polymer emulsions. Cem. Concr. Compos. 157, 105910. https://doi.org/10.1016/j.cemconcomp.2024.105910.

Zhang, X.M., Jiang, G.C., Dong, T.F., et al., 2018. An amphoteric polymer as a shale borehole stabilizer in water-based drilling fluids. J. Pet. Sci. Eng. 170, 112–120. https://doi.org/10.1016/j.petrol.2018.06.051.

Zhang, Y., Ding, C., Zhang, N., et al., 2024. Contributions of TCA-KTTO-modified quartz tailings and CPE toughener in PVC composites to enhance the mechanical-thermal performance. Chem. Eng. J. 495, 153166. https://doi.org/10.1016/j.cej.2024.153166.

Zhao, X., Qiu, Z.S., Sun, B.J., et al., 2019. Formation damage mechanisms associated with drilling and completion fluids for deepwater reservoirs. J. Pet. Sci. Eng. 173, 112–121. https://doi.org/10.1016/j.petrol.2018.09.098.